



## Determining Electromagnetic Energy Resolution of a Combined GdTaO<sub>4</sub> Crystal-Photodetector System with a Simulation Study

Ali ÖZTÜRK<sup>1,2</sup>, Gural AYDIN<sup>1\*</sup>

<sup>1</sup> Hatay Mustafa Kemal University, Faculty of Arts and Science, Department of Physics, Hatay, Turkey

<sup>2</sup> now at, Turkish Red Crescent Community Center, 33070, Akdeniz/Mersin, Turkey

Ali ÖZTÜRK ORCID No: 0000-0002-1404-6515

Gural AYDIN ORCID No: 0000-0002-4996-1174

\*Corresponding author: [gaydin@mku.edu.tr](mailto:gaydin@mku.edu.tr)

(Alınış: 09.11.2020, Kabul: 18.03.2021, Online Yayınlanma: 25.06.2021)

### Keywords

Energy resolutions, Geant4, High density scintillator, Homogeneous electromagnetic calorimeter

**Abstract:** Scintillators used as active materials of calorimeters play an important role in particle physics experiments. The optical, scintillating and physical properties of scintillation materials affect performances of calorimeters significantly. In this work, GdTaO<sub>4</sub> crystal with very high density was examined as an active material in a homogenous calorimeter using Geant4 simulation code. This paper presents the results of the electromagnetic performances of a homogenous calorimeter with active material of GdTaO<sub>4</sub>. The calorimeter modules were reconstructed in the simulation program in different geometries and energy resolution values for various scintillator-photodetector combinations were obtained as a function of incident gamma beam energies. The predictions of the improvements in energy resolutions with the interested scintillator-photodetector combinations compared to previous studies were noted.

## Birleşik GdTaO<sub>4</sub> Kristal-Foto Detektör Sistemi için Elektromanyetik Enerji Çözünürlüğünün Benzetim Çalışması ile Belirlenmesi

### Anahtar Kelimeler

Enerji çözünürlüğü, Geant4, Yüksek yoğunluklu sintilatör, Homojen elektromanyetik kalorimetresi

**Öz:** Kalorimetrelerin aktif malzemesi olarak kullanılan sintilatörler parçacık fiziği deneylerinde önemli rol oynamaktadır. Bu sintilasyon malzemelerinin optik, ışıltama ve fiziksel özellikleri kalorimetrelerin performansını önemli derecede etkilemektedir. Bu çalışmada, yüksek yoğunluklu GdTaO<sub>4</sub> kristali, bir homojen kalorimetrenin aktif malzemesi olarak Geant4 benzetim programını kullanarak incelenmiştir. Bu makale, aktif malzemesi GdTaO<sub>4</sub> olan bir homojen kalorimetresinin elektromanyetik performansını sunmaktadır. Benzetim programında kalorimetre modülü farklı geometrilerde inşa edilmiş ve gama ışını enerjilerine bağlı olarak farklı sintilatör-fotodetektör birleşimleri için enerji çözünürlüğü değerleri elde edilmiştir. Enerji çözünürlüklerindeki daha önce yapılan çalışmalara oranla öngörülen ilerlemeler not edilmiştir.

### 1. INTRODUCTION

Homogenous calorimeters used in particle physics experiments are designed solely with a scintillation material mainly to measure energy and direction of incident particles. The properties of scintillators affect performances of homogenous electromagnetic calorimeters in terms of scintillator-photodetector combinations in high energy and particle physics experiments. For example, the light yield of a scintillation material is an important factor to achieve required energy resolutions related to the photoelectron

statistics. Scintillation decay times in scintillators and signal formation in photodetectors should be fast enough for satisfying data taking rate. On the other hand, density of a scintillation material is very important factor for constructing compact calorimeters and having better spatial and energy resolutions since high density scintillators produce well defined light bursts. Since homogenous calorimeters uses long scintillators, self-absorption of the scintillators could be seriously effective in light collection at the photodetectors. If there is no self-absorption in the scintillator, measured transmission spectra of a given scintillator will be close to theoretical transmission limits which consider

multiple bounces of photons between two parallel ends. Another factor affecting the calorimeter performance is how well emission spectra of the emitted lights in the scintillator matches with photodetector's spectral response range and quantum efficiencies. Recently, PIN photodiodes and avalanche photodiodes (APD) were used in particle physics experiments: Hamamatsu S2744-08 PIN diode as the photodetector was used in BesIII [1], Babar [2], and BELLE [3] experiments. APD S8664-55 was used in Compact Muon Selenoid (CMS) experiment at CERN [4] with PWO crystals. The quantum efficiencies of the Silicon photodiodes (SPDs) are higher at relatively high wavelengths compared to those for the conventional photo multiplier tubes (PMT). This was one of the main reasons that recent experiments used SPDs with appropriate scintillators. Generally, SPDs have broad spectral range from infrared to high energy regions. They have high-speed response, high sensitivity, high stability, and low noise [5]. APD is suitable in the case of low light yield since it produces high current in short time. This is one of the main reasons to be used with PWO crystals for the electromagnetic calorimetry in the CMS experiment [6, 7].

The main focus of this study is to search how high density scintillator material could allow more compact calorimeter and achieving high energy resolutions. The material which was examined as the active material of a homogenous calorimeter is GdTO<sub>4</sub>, which is a scintillator with the highest density (8.94 g/cm<sup>3</sup>) among current scintillators. It was grown by Czochralski method and reported that the high quality and bulk single crystal of GdTO<sub>4</sub> was first grown [8, 9]. Its pulse-height measurement, scintillation decays, thermal and hardness properties were also reported [8, 9]. Before that study, the growth of the crystal were either with inclusion and twins or were of small size which was not large enough for scintillation measurements. Its attenuation length has been reported to be 1 cm, which is second to PWO [10, 11]. GdTO<sub>4</sub> has transmission spectra indicating that it has no significant self-absorption within its emission spectra ranging from 400 nm to 700 nm peaking at 541 nm. It was shown that its scintillation light yield is about three times that of PWO whose light yield is 120 photons/MeV [12, 13]. Its scintillation fast and slow decay time constants were reported as 72.6 ns and 1236.2 ns, respectively [9]. It appears that the main drawback of the interested scintillator is its slow decay component. Future studies for understanding the luminescence mechanism of the material may eliminate this drawback. GdTaO<sub>4</sub> is a crystal which has not been used so far in particle physics experiments in a calorimeter or its simulation study regarding to the electromagnetic performances has not been presented to the best of our knowledge. This study aimed to determine energy resolutions of a homogenous calorimeter consisting of promising GdTaO<sub>4</sub> scintillator in different sizes as scintillator-photodetector combinations. The study was performed with Geant4 [14-16] simulation program and experimental results of the scintillation and optical properties were used in the calculations leading to the energy resolution parametrization.

## 2. MATERIAL AND METHOD

The first contribution to the total energy resolution is the shower fluctuation with energy leakage out of detector volume which mainly depends on material itself and detector geometry. This effect will manifest as energy fluctuations deposited in a scintillation material. The second one is photoelectron statistics contribution regarding to the number of produced primary photoelectrons in photodetectors coupled to scintillators. Photodetector signal fluctuations will be related to the photoelectron statistics. The photoelectron statistics mainly depends on light yield of a scintillator material, photon transmission in the material through the photodetectors, and photodetector quantum efficiency as a function of scintillation emission spectrum. Another possible factor which could affect the energy resolution is the electronic noise that is defined as signal production in photodetectors without any incident beam on the detector. This factor will strongly depend on electronics in signal readout. On the other hand, some experimental techniques such as applying energy threshold for the calorimeters could reduce electronic noise contribution significantly.

In this study, the contribution to the energy resolution due to fluctuation in electromagnetic shower containment were determined by fitting the energy deposition distributions with the function shown by Equation 1 [17]. The energy deposition distribution were obtained with Geant4 (Geometry and Transportation) simulation program in which the physics list of standard electromagnetic process was selected. The related distributions were obtained for several detector geometries as a function of incident beam energies.

$$F(x) \equiv N \exp \left( -\frac{1}{2\sigma_0^2} \ln^2 \left( 1 - \frac{x - x_p}{\sigma_E} \eta \right) - \frac{\sigma_0^2}{2} \right) \quad (1)$$

where  $\sigma_0 = 2/\xi \sinh^{-1}(\eta\xi/2)$  and  $\xi = 2\sqrt{\ln 4}$ . Here,  $x_p$  is the peak value and  $\eta$  is defined as the asymmetry parameter which measures the tail occurring at lower edges in the energy deposition distributions,  $N$  is the normalization factor, and  $\sigma_E$  is the full width at half maximum (FWHM) divided by  $\xi$ . In this case, the energy resolution is determined taking the ratio of  $\sigma_E$  to  $x_p$ . A Typical fit belonging to the distribution for 1 GeV gamma beam on the scintillator with 100 mm x 100 mm transverse size and 20 cm thickness is shown in Figure 1.

The intrinsic energy resolutions were determined for various incident gamma beam energies between 100 MeV to 2 GeV. Numerous detector geometries were built in the simulation program, which could be considered in the matrix forms of 3 x 3, 4 x 4, and 5 x 5 scintillator slabs. Each scintillator slab has the transverse size of 20 mm x 20 mm and the thicknesses of the slabs were arranged in three lengths of 16 cm, 18 cm, and 20 cm. In this way, nine geometric configurations were simulated within the program. In this setup, the detector

module has the transverse sizes of 60 mm x 60 mm, 80 mm x 80 mm, or 100 mm x 100 mm.

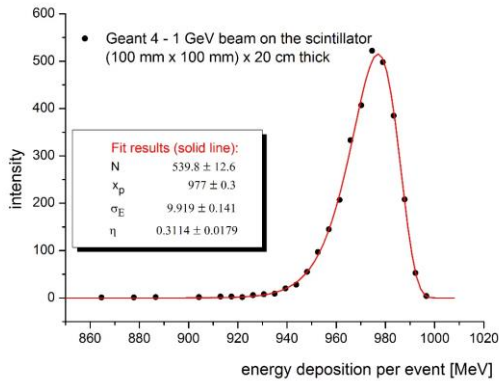


**Figure 1.** Energy deposition distribution with fit the function (solid line). 1 GeV incident gamma beam on GdTaO<sub>4</sub>.

The detector intrinsic resolutions (energy leakage contribution) were determined by fitting the energy deposition distributions with the function given with Equation 1. It was figured out that these energy resolutions follow quite well with beam energies with the function given by Equation 2.

$$\frac{\sigma(E)}{E} = \frac{a_{lateral}}{E^{1/4}} \oplus b \quad (2)$$

The symbol indicates a quadratic summation of neighboring items. Mainly, the energy leakage in transverse direction is represented with  $a_{lateral}$  and the leakage in the longitudinal direction appears in constant term.

Photodetector signal fluctuation contributes to the total energy resolution regarding to the number of produced primary photoelectrons and emission weighted excess noise factor which is related to the internal gain fluctuation. The photoelectron statistics term  $a_{pe}$  is determined with Equation 3 [6].

$$a_{pe} = \sqrt{\frac{\bar{F}}{N_{pe}}} \quad (3)$$

In the formula,  $\bar{F}$  refers to the emission weighted excess noise factor and  $N_{pe}$  refers to the number of primary photoelectrons produced at the photodetector for per GeV incident beam energy. Two types of photodetectors were considered in this study: a PIN diode and an APD. The spectral ranges for the APD S8664-55 and pin diode S2744-08 are reported between 320- 1100 nm, 340-1100 nm, respectively [5]. They well match with the emission spectra of the interested material. In this study,  $\bar{F}$  was determined as 3.1 for APD by taking account of wavelength dependent excess noise factor for the APD structure at the constant gain value of 50 [18]. Since PIN diodes have no internal gain, this value was taken as 1 in this case. The average number of primary photoelectrons was estimated by taking account of the material's average light yield and transmission spectra, photodetector emission weighted quantum efficiencies

and photodetector active area compared to the scintillator back face area. Since APD used in this study has much less size than PIN and it has excess noise factor, it will contribute to the energy resolution significantly. The ratios of the PIN and APD active areas to the area of the scintillator cross section were 1 and 0.125, respectively considering that each scintillator includes two photodetectors at rear face. The emission weighted quantum efficiencies were determined as 84% and 79% for APD and PIN photodetectors, respectively. These efficiencies were calculated by considering both emission spectrum of the scintillator [8] and quantum efficiencies of the photodetectors as a function of wavelength [5]. In this way, emission weighted quantum efficiencies were determined for each photodetector. The average scintillation light yield was taken as 360 photons/MeV in the calculations. The photostatistics term,  $a_{pe}$ , was determined for the detector geometries of 100 mm x 100 mm in transverse size and thicknesses of 20 cm and 18 cm in the unit of  $\text{GeV}^{1/2}$  as 0.22 % and 1.04 % for PIN and APD, respectively. This fluctuation contributes to the total energy resolution with the function of type  $(a_{pe}/\sqrt{E})$ , where is in GeV unit.

Previous studies showed that this type of simulation gives consistent results with experimental data and the estimation of the average number of photoelectrons has been reported reasonable when it is compared with experimental results by taking account of detector geometries [19, 20].

### 3. RESULTS AND DISCUSSION

Figures 2-4 shows the intrinsic energy resolution results for certain calorimeter thicknesses with different transverse sizes. The common property of these figures is that at lower beam energies, the transverse size becomes more effective and so the resolutions varies significantly with transverse sizes for a constant calorimeter thickness. Figures 5-7 shows the energy resolutions for the same transverse sizes to compare the results belonging to the different calorimeter thicknesses. It could be said that the resolutions varies more with calorimeter thicknesses at the larger transverse sizes especially for those with the 100 mm x 100 mm transverse area. The intrinsic resolutions reach the values of 1.67, 1.40, and 1.14% for the calorimeter with 80 mm x 80 mm transverse size and 18 cm thickness at the beam energies of 0.6, 1, and 2 GeV, respectively. For the calorimeter whose transverse size is 100 mm x 100 mm and thickness 18 cm, the resolutions are seen to be 1.29, 1.14, and 0.97% belonging to the beam energies of 0.6, 1, and 2 GeV, respectively. The energy resolution values reach 1.55, 1.31, and 0.99% for the calorimeter with 80 mm x 80 mm transverse size and 20 cm thickness at the beam energies of 0.6, 1, and 2 GeV, respectively. For the calorimeter whose transverse size is 100 mm x 100 mm and thickness is 20 cm, the resolutions were determined as 1.19, 1.02, and 0.82% belonging to the beam energies of 0.6, 1, and 2 GeV, respectively. It is seen that the results belonging to even 80 mm x 80 mm transverse size and thicknesses of 18 cm and 20 cm are very good

and the results for the calorimeter geometry of having 100 mm x 100 mm transverse size reach excellent values at both 18 cm and 20 cm thicknesses.

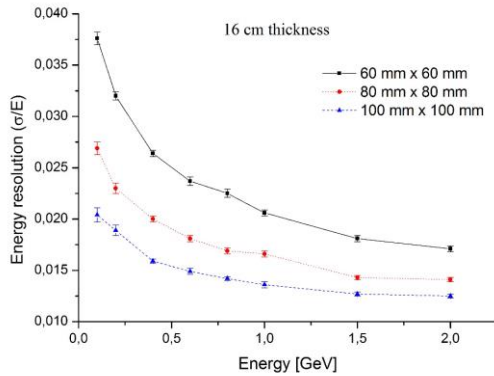


**Figure 2.** Intrinsic energy resolutions in terms of incident beam energies for 16 cm calorimeter thickness and various calorimeter transverse sizes.

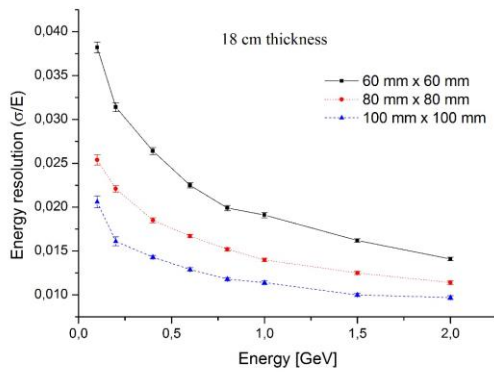


**Figure 3.** Intrinsic energy resolutions in terms of incident beam energies for 18 cm calorimeter thickness and various calorimeter transverse sizes.

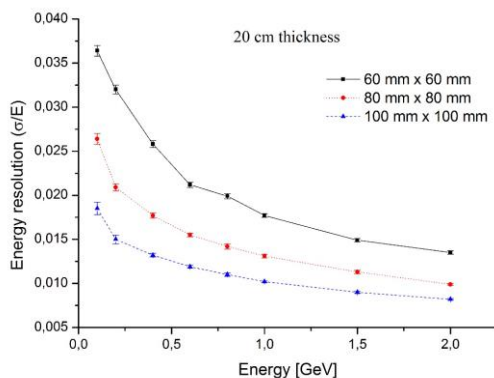


**Figure 4.** Intrinsic energy resolutions in terms of incident beam energies for 20 cm calorimeter thickness and various calorimeter transverse sizes.

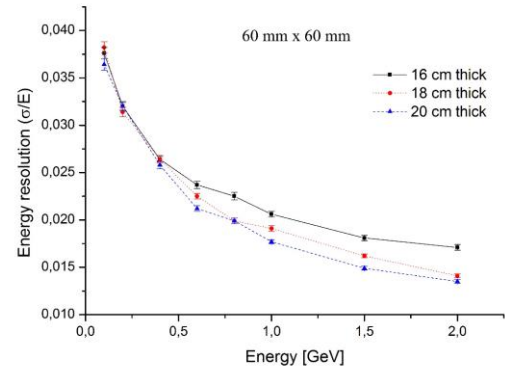


**Figure 5.** Intrinsic energy resolutions in terms of incident beam energies for 60 mm x 60 mm calorimeter transverse size and various calorimeter thicknesses.

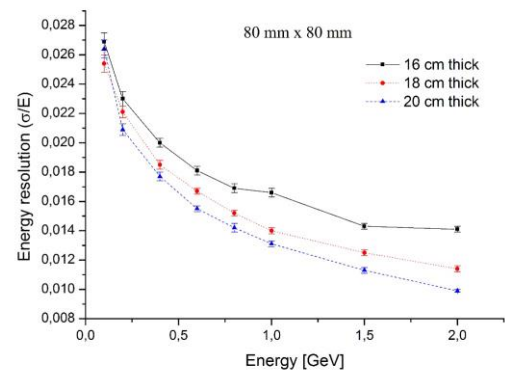


**Figure 6.** Intrinsic energy resolutions in terms of incident beam energies for 80 mm x 80 mm calorimeter transverse size and various calorimeter thicknesses.

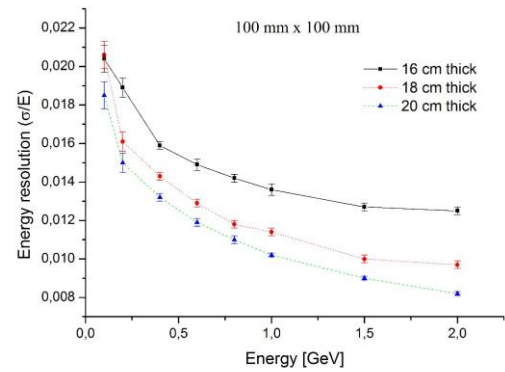


**Figure 7.** Intrinsic energy resolutions in terms of incident beam energies for 100 mm x 100 mm calorimeter transverse size and various calorimeter thicknesses.

The parametrized energy resolutions were determined for the calorimeter geometries of 100 mm x 100 mm in transverse size and for 18 cm and 20 cm thicknesses. The intrinsic energy resolutions were fitted with the function given in Equation 2. Figure 8 shows the resolutions with the fit functions. In this way, the fit results gave the lateral and constant terms of the total energy resolution function in addition to the photoelectron statistics terms. The total energy resolutions were then calculated as the quadratic summation of each contributing term. The parametrized

energy resolution functions are shown with two types of photodetectors in Equations 4-7. The total energy resolution functions for scintillator-photodetector combinations were drawn with the obtained parametrized functions and shown in Figure 9 and Figure 10. It is obviously seen that the resolutions with APD are significantly lower compared to that of PIN diode especially at relatively low beam energies as it is expected due to their smaller sizes and excess noise factor which contribute to the photoelectron statistics term. It can be said that even with this photodetector size, the results with APD are reasonable.

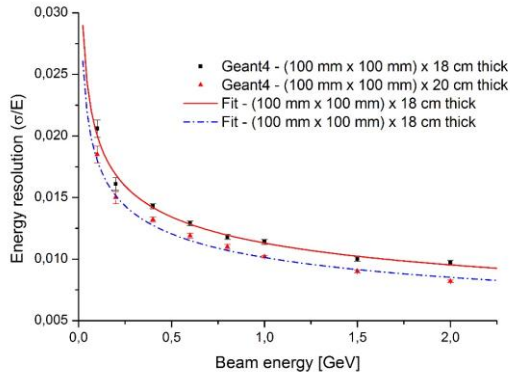


**Figure 8.** Fit functions (solid lines) applied for the intrinsic energy resolutions shown with markers.

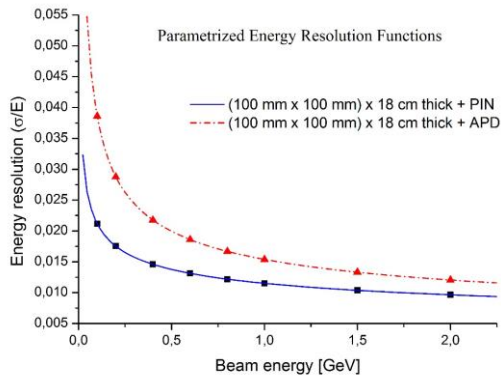


**Figure 9.** Parametrized energy resolution functions (dotted lines) with APD and PIN for the calorimeter with 100 mm x 100 mm transverse size and 18 cm thickness. Markers refer to points in the fit functions.

$$\sigma/E = 1.12\%/E^{1/4} \oplus 1.04\%/\sqrt{E} \oplus 0.12\% \quad (4)$$

for (100 mm x 100 mm) x 18 cm + APD

$$\sigma/E = 1.12\%/E^{1/4} \oplus 0.22\%/\sqrt{E} \oplus 0.12\% \quad (5)$$

for (100 mm x 100 mm) x 18 cm + PIN

$$\sigma/E = 1.01\%/E^{1/4} \oplus 1.04\%/\sqrt{E} \oplus 7.29 \times 10^{-14}\% \quad (6)$$

for (100 mm x 100 mm) x 20 cm + APD

$$\sigma/E = 1.01\%/E^{1/4} \oplus 0.22\%/\sqrt{E} \oplus 7.29 \times 10^{-14}\% \quad (7)$$

for (100 mm x 100 mm) x 20 cm + PIN

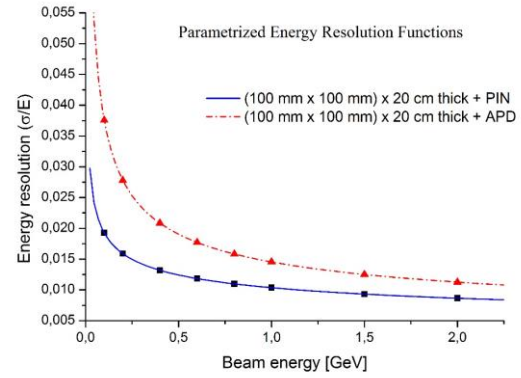


**Figure 10.** Parametrized energy resolution functions with APD and PIN for the calorimeter with 100 mm x 100 mm transverse size and 20 cm thickness. Markers refer to points in the fit functions.

GdTaO<sub>4</sub> has similar density and average light yield with PWO. It can be said that even smaller sizes of the interested material gives compatible results with those of PWO and significant improvements are predicted with the same detector geometry [19]. For example, at 100 MeV beam energy, PWO+APD gives roughly 6% energy resolution at [19]. This study gives better than 4% resolution at the same beam energy and APD combination.

Finally, contributions to total energy resolutions were drawn separately in Figures 11 and 12. in the case of APD or PIN as a photodetector considering the scintillator geometry of 100 mm x 100 mm in transverse size and 20 cm in thickness. In the figures, the parametrized intrinsic energy resolutions were defined as the energy leakage contribution to the total energy resolution. In the case of APD, the photoelectron statistics contribution dominate below 1 GeV beam energy essentially up to around 0.5 GeV and this effect decreases with beam energy as expected. On the other hand, in the case of PIN, energy leakage contribution dominates at all beam energies. In this case, the contribution from photoelectron statistics is very limited.

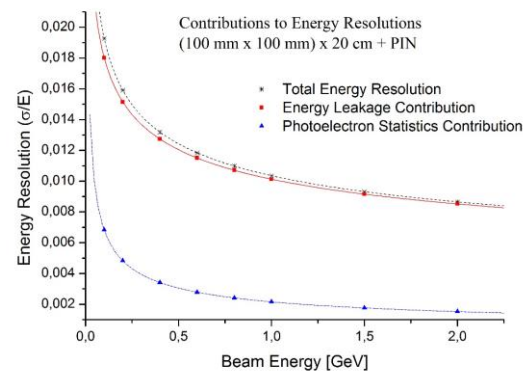


**Figure 11.** Contributions to total energy resolution for scintillator-PIN combination. The total energy resolution was determined by taking the quadratic summation of each contributing term.

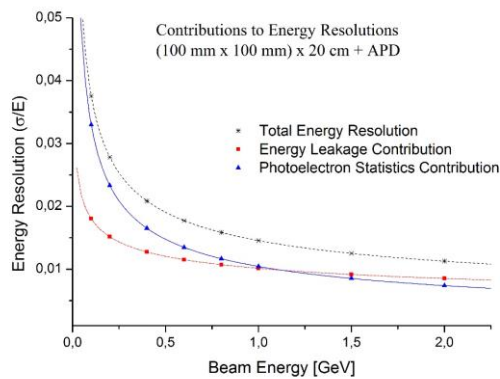


**Figure 12.** Contributions to total energy resolution for scintillator-APD combination. Total energy resolution again was determined by taking the quadratic summation of each contributing term.

#### 4. CONCLUSION

High-density scintillation materials is an important factor essentially for constructing more compact detectors or increasing the energy resolutions. This study aimed to show that higher density of scintillators has a considerable effect on the energy resolution of calorimeters. GdTaO<sub>4</sub> was considered as an active material of a homogenous calorimeter assembling in scintillator-photodetector combinations with PIN or APD. Two major contribution to total energy resolution were considered: Energy deposition fluctuation and photoelectron statistics contribution related to the photodetector signal fluctuation. In this study, we haven't taken account of any possible inhomogeneity due to light collection and electronic noise contribution. The intrinsic energy resolutions which are very close to or below 1% due to energy deposition fluctuations are predicted at some beam energies in a given energy range and for certain detector geometries. It was noticed that parametrized energy resolution function has negligible constant term with the detector geometry of 100 mm x 100 mm in transverse size and 20 cm in thickness. This term has very small contribution in the case of detector geometry whose length is 18 cm with 100 mm x 100 mm transverse size. This term will also originate from systematic uncertainties in a real experiment. The advantages of GdTaO<sub>4</sub> compared to PWO, which has higher light yield and higher density, can make significant improvements in energy resolutions when used with an APD photodetector. The presented results are showing that GdTaO<sub>4</sub> has capability achieving good energy resolution results when it is used with both APD and PIN even at relatively low beam energies below 1 GeV with suitable scintillator-photodetector combinations.

#### REFERENCES

[1] Ablikim M, An ZH, Bai JZ, Berger N, Bian JM, Cai X, et al. Design and construction of the Belle II detector. *Nuclear Instruments and Methods in Physics Research Section A*. 2010; 614(3):345-399.

[2] Lewandowski B, for the BaBar EMC Group. The BaBar electromagnetic calorimeter. *Nuclear*

*Instruments and Methods in Physics Research Section A*. 2002; 494(1-3):303-307.

[3] Miyabayashi K, for the Belle Electromagnetic Calorimeter Group. Belle electromagnetic calorimeter. *Nuclear Instruments and Methods in Physics Research Section A*. 2002; 494(1-3):298-302.

[4] Renker D. Properties of avalanche photodiodes for applications in high energy physics, astrophysics and medical imaging. *Nuclear Instruments and Methods in Physics Research Section A*. 2002; 486(1-2):164-169.

[5] Hamamatsu Photonics [Internet]. Photodiodes; 2018 [cited 2018 March 05]. Available from <https://www.hamamatsu.com/jp/en/product/optical-sensors/photodiodes/index.html>.

[6] Chatrchyan S, Hmayakyan G, Khachatryan V, Sirunyan AM, Adam W, CMS Collaboration, et al. The CMS experiment at the CERN LHC. *Journal of Instrumentation*. 2008; 3:S08004.

[7] Paramatti R, on behalf of the CMS Collaboration. Design options for the upgrade of the CMS electromagnetic calorimeter. *Nuclear and Particle Physics Proceedings*. 2016; 273-275:995-1001.

[8] Liu W, Zhang Q, Zhou W, Gu C, Yin S. Growth and Luminescence of M-Type GdTaO<sub>4</sub> and Tb:GdTaO<sub>4</sub> Scintillation Single Crystals. *IEEE Transactions on Nuclear Science*. 2010; 57(3):1287-1290.

[9] Yang H, Peng F, Zhang Q, Guo C, Shi C, Liu W, et al. A promising high-density scintillator of GdTaO<sub>4</sub> single crystal. *CrystEngComm*. 2014; 16(12):2480-2485

[10] Lecoq P, Dafinei I, Auffray E, Schneegans M, Korzhik MV, Missevitch OV, et al. Lead tungstate (PbWO<sub>4</sub>) scintillators for LHC EM calorimetry. *Nuclear Instruments and Methods in Physics Research Section A*. 1995; 365(2-3):291-298.

[11] Moses WW, Weber MJ, Derenzo SE, Perry D, Berdahl P, Boatner LA. Prospects for dense, infrared emitting scintillators. *IEEE Trans. Nucl. Sci.* 1998; 45(3):462-466.

[12] Alexeev GA, Binon F, Dolgoplov AV, Donskov SV, Fyodorov AA, Kachanov VA, et al. Beam test results of a PbWO<sub>4</sub> crystal calorimeter prototype. *Nuclear Instruments and Methods in Physics Research Section A*. 1995; 364(2):307-310.

[13] Novotny R, Doring W, Mengel K, Metag V, Pienne C. Response of a PbWO<sub>4</sub>-scintillator array to electrons in the energy regime below 1 GeV. *IEEE Transactions on Nuclear Science*. 1997; 44(3):477-483.

[14] Agostinelli S, Allison J, Amako K, Apostolakis J, Araujo H, Arce P, et al. Geant4—a simulation toolkit. *Nuclear Instruments and Methods in Physics Research Section A*. 2003; 506(3):250-303.

[15] Allison J, Amako K, Apostolakis J, Araujo H, Arce P, Asai M, et al. Geant4 developments and applications. *IEEE Transactions on Nuclear Science*. 2006; 53(1):270-278.

[16] Allison J, Amako K, Apostolakis J, Arce P, Asai M, Aso T, et al. Recent developments in Geant4.

- Nuclear Instruments and Methods in Physics Research Section A. 2016; 835:186-225.
- [17] Ikeda H, Satpathy A, Ahn BS, Aulchenko VM, Bondar AE, Cheon BG, et al. A detailed test of the CsI (Tl) calorimeter for BELLE with photon beams of energy between 20 MeV and 5.4 GeV. Nuclear Instruments and Methods in Physics Research A. 2000; 441(3):401-426.
- [18] Pilicer E, Kocak F, Tapan I. Excess noise factor of neutron-irradiated silicon avalanche photodiodes. Nuclear Instruments and Methods in Physics Research Section A. 2005; 552(1-2):146-151
- [19] Kocak F. Simulation studies of crystal-photodetector assemblies for the Turkish accelerator center particle factory electromagnetic calorimeter. Nuclear Instruments and Methods in Physics Research A. 2015; 787:144–147.
- [20] Kocak F, Tapan I. Simulation of LYSO Crystal for the TAC-PF Electromagnetic Calorimeter. ACTA PHYSICA POLONICA A. 2017; 131(3):527-529.